Final Technical Report

Growth, Characterization and Device Development in Monocrystalline Diamond Films

Supported under Grant #N00014-93-I-0437
Office of the Chief of Naval Research
Report for the period 1/1/98–3/31/98

R. F. Davis, R. J. Nemanich* and Z. Sitar
P. K. Baumann*, M. J. Benjamin*, S. L. English*, S. K. Han,
J. D. Hartman, B. L. McCarson, M. T. McClure, R. Schlesser,
A. T. Sowers*, and B. L. Ward*
North Carolina State University
c/o Materials Science and Engineering Department
*Department of Physics
Box 7907
Raleigh, NC 27695

March, 1998

REPORT DOCUMENTATION PAGE

Form Approved
OMB No. 0704-0188

1. AGENCY USE ONLY *(Leave blank)*	2. REPORT DATE	3. REPORT TYPE AND DATES COVERED
	March, 1998	Final Technical 1/1/98–3/31/98

4. TITLE AND SUBTITLE

Growth, Characterization and Device Development in Monocrystalline Diamond Films

5. FUNDING NUMBERS

s400003srr14
1114SS
N00179
N66005
4B855

6. AUTHOR(S)

R. F. Davis, R. J. Nemanich, and Z. Sitar

7. PERFORMING ORGANIZATION NAME(S) AND ADDRESS(ES)

North Carolina State University
Hillsborough Street
Raleigh, NC 27695

8. PERFORMING ORGANIZATION REPORT NUMBER

N00014-93-I-0437

9. SPONSORING/MONITORING AGENCY NAMES(S) AND ADDRESS(ES)

Sponsoring: ONR, Code 312, 800 N. Quincy, Arlington, VA 22217-5660
Monitoring: Admin. Contracting Officer, Office of Naval Research
Atlanta Regional Office
100 Alabama Street, Suite 4R15
Atlanta, GA 30303

10. SPONSORING/MONITORING AGENCY REPORT NUMBER

11. SUPPLEMENTARY NOTES

12a. DISTRIBUTION/AVAILABILITY STATEMENT

Approved for Public Release; Distribution Unlimited

12b. DISTRIBUTION CODE

13. ABSTRACT ***(Maximum 200 words)***

Surfaces of diamond and GaN have been characterized using UV photoemission spectroscopy (UPS), position dependent field emission and photo-electron emission microscopy (FEEM and PEEM). Electron affinity is a critical limiting aspect for field emission from conducting p-type diamond and Si doped GaN. Emission from p-type diamond originates from the valence band of the material; field emission from Si-doped GaN originates from electrons in the conduction band. Particle detectors for high electron flux applications have been fabricated based on highly oriented diamond (HOD) films. Relatively thick HOD films were achieved by combining the bias enhanced nucleation in a microwave plasma chemical vapor deposition reactor and high rate growth process in a low pressure combustion flame reactor. The detector performance was measured using the energy spectra of alpha-particles emitted from an ^{241}Am source. The HOD detector showed a three to four fold improvement in performance which was close to that obtained for single crystalline diamond detectors. Voltage-dependent field emission energy distribution and I-V measurements were performed on Mo tips coated with intrinsic c-BN to determine the origin of the field-emitted electrons. Spectra were collected from the Mo emitters under UHVconditions before and after being coated. In some instances multiple FEED peaks were observed in the collected spectra. These corresponded to multiple emission sites on the emitter. The energy of the field-emitted electrons from the c-BN-coated emitters usually depended linearly upon the applied voltage and could be explained using a simplified band-bending model. However, at higher voltages the FEED measured from the c-BN-coated emitters departed from this linear behavior. These nonlinearities were attributed to contact resistance at the Mo/c-BN interface.

14. SUBJECT TERMS

diamond, gallium nitride, GaN, UV photoemission spectroscopy, UPS, position dependent field emission and photo-electron emission microscopy, electron affinity, highly oriented diamond films, field emission, energy distribution, c-BN, boron nitride

15. NUMBER OF PAGES

34

16. PRICE CODE

17. SECURITY CLASSIFICATION OF REPORT	18. SECURITY CLASSIFICATION OF THIS PAGE	19. SECURITY CLASSIFICATION OF ABSTRACT	20. LIMITATION OF ABSTRACT
UNCLAS	UNCLAS	UNCLAS	SAR

Table of Contents

I. Introduction

Diamond as a semiconductor in high-frequency, high-power transistors has unique advantages and disadvantages. Two advantages of diamond over other semiconductors used for these devices are its high thermal conductivity and high electric-field breakdown. The high thermal conductivity allows for higher power dissipation over similar devices made in Si or GaAs, and the higher electric field breakdown makes possible the production of substantially higher power, higher frequency devices than can be made with other commonly-used semiconductors.

In general, the use of bulk crystals severely limits the potential semiconductor applications of diamond. Among several problems typical for this approach are the difficulty of doping the bulk crystals, device integration problems, high cost and low area of such substrates. In principal, these problems can be alleviated via the availability of chemically vapor deposited (CVD) diamond films. Recent studies have shown that CVD diamond films have thermally activated conductivity with activation energies similar to crystalline diamonds with comparable doping levels. Acceptor doping via the gas phase is also possible during activated CVD growth by the addition of diborane to the primary gas stream.

The recently developed activated CVD methods have made feasible the growth of polycrystalline diamond thin films on many non-diamond substrates and the growth of single crystal thin films on diamond substrates. More specifically, single crystal epitaxial films have been grown on the {100} faces of natural and high pressure/high temperature synthetic crystals. Crystallographic perfection of these homoepitaxial films is comparable to that of natural diamond crystals. However, routes to the achievement of rapid nucleation on foreign substrates and heteroepitaxy on one or more of these substrates has proven more difficult to achieve. This area of study has been a principal focus of the research of this contract.

At present, the feasibility of diamond electronics has been demonstrated with several simple experimental devices, while the development of a true diamond-based semiconductor materials technology has several barriers which a host of investigators are struggling to surmount. It is in this latter regime of investigation that the research described in this report addresses.

In this reporting period, (1) surfaces of diamond and GaN have been characterized using UV photoemission spectroscopy (UPS), position dependent field emission and photo-electron emission microscopy (FEEM and PEEM); (2) particle detectors for high electron flux applications were fabricated based on highly oriented diamond (HOD) films and characterized; and (3) voltage-dependent field emission energy distribution and I-V measurements were performed on Mo tips coated with intrinsic c-BN to determine the origin of the field-emitted electrons. The following sections are self-contained in that they present an introduction, experimental procedures, results and discussion, summary and indications of future research for the given research thrust.

II. Characterization of Electron Emitting Surfaces of Diamond and III-V Nitrides

R. J. Nemanich, P.K. Baumann, M.J. Benjamin, S.L. English, J.D. Hartman,
A.T. Sowers, B.L. Ward
Department of Physics and Department of Materials Science and Engineering
North Carolina State University, Raleigh, NC 27695-8202

Wide bandgap semiconductors such as diamond and the diamond related materials of GaN and AlN, exhibit small or even negative electron affinities. Recent results have shown that surface treatments will modify the electron affinity of diamond to cause a negative electron affinity (NEA). For the III-V nitrides of GaN and AlN, results indicate a NEA for some surfaces of AlN and an electron affinity of 3.3 eV for GaN. Alloys of AlGaN exhibit a composition dependent electron affinity which trends to a value of zero at ~70% AlN. This study describes the characterization of these surfaces using UV photoemission spectroscopy (UPS), position dependent field emission and photo-electron emission microscopy (PEEM). Results are summarized which correlate the field emission from single crystal p-type (boron doped) diamond with various surface processes used to establish a NEA surface. The field emission threshold from the nitrogen doped samples is significantly higher than from p-type diamond, and in fact, most surfaces are severely damaged during the emission measurement. The PEEM technique, which combines aspects of UPS and field emission, images the emitted electrons allowing a true relation of the emission to the surface morphology. PEEM results are presented for both diamond and nitride surfaces.

Contact Author:
Robert J. Nemanich
Department of Physics
North Carolina State University
Raleigh, NC 27695-8202
USA

Phone: (919) 515-3225
FAX: (919) 515-7331
Email: Robert_Nemanich@ncsu.edu

Submitted to Diamond Films and Technologies, March 1998

Introduction

Electron emission from wide bandgap semiconductors offers the potential for cold cathode structures which would have a wide range of applications. Common semiconductors are based on sp^3 type bonding, and the incorporation of impurities can lead to p- or n-type doping characteristics. The discovery of a high quantum yield for photo-electron emission from diamond (111) surfaces indicated the potential for diamond as an electron emitter [1]. It was later concluded that the diamond (111) surface, when terminated with hydrogen exhibits a negative electron affinity [2].

The property of a negative electron affinity will allow conduction band electrons to be freely emitted from a surface into vacuum without a barrier. Hence, the electron affinity of wide bandgap semiconductors has been the focus of many studies. However, the development of cold cathode devices will require emission without the assistance of light. Thus, field emission of wide bandgap semiconductors has also been studied as a validation of the materials properties required to fabricate cold cathode structures. While many investigators have employed field emission and photoemission to characterize surfaces, there have been significant differences in reports of similar materials. This study explores the characterization of electron emission characteristics of wide bandgap materials. In particular, photoemission results are summarized and correlated with field emission results. Moreover, we present photoelectron emission measurements which help display the point of origin of the electron emission.

The materials of diamond, boron nitride, SiC, Al-Ga-In nitrides and their alloys are often considered in the group of diamond-type materials because of their strong bonding leading to hard materials. These materials are stable for relatively high temperature operation, and they resist defect formation and dopant diffusion. With these characteristics, they have been considered as a group for high power applications. With regards to field emission applications these same properties will be important for high current emission and a resistance to sputtering induced degradation.

While the ideal cold cathode material would exhibit a negative electron affinity as noted above, other properties are equally if not more important. The supply of electrons to the emitting surface will require a low resistance ohmic contact and transport of the electrons through the semiconducting material. To achieve these properties, n-type semiconducting characteristics may be required. Highly doped n-type material will allow low resistance contacts and provide electrons for transport through the material.

Field emission characterization of materials involves all of the attributes noted above. In fact, there are often many possible emission mechanisms so that it is sometimes impossible to determine the appropriate process for a single field emission measurement. In this study, we describe how photoemission and field emission techniques can be applied for the

characterization of electron emission materials, and we summarize recent results on the diamond-type, hard, wide bandgap semiconductors. In a unique combination of the two techniques, we describe how photo-electron emission microscopy (PEEM) can be employed to relate the two processes and to determine the spatial characteristics of the electron emission.

Experimental Procedure

In this study, measurements are presented for diamond and nitride surfaces. The samples include 3mm x 3mm x 0.25mm type IIb natural diamonds, boron or nitrogen doped microwave plasma CVD diamond films, epitaxial AlGaN films, and Si doped GaN pyramid structures prepared by selective OMCVD growth processes.

For the photoemission measurements presented here, the spectra were excited with HeI radiation (21.2 eV), and the electrons were energy analyzed with a VSW 50mm mean radius hemispherical electron analyzer. All the measurements presented here were obtained for surface normal emission.[3]

The photoemission spectrum exhibits two aspects which indicate that the surface exhibits a negative electron affinity [2, 3]. The first is the presence of a strong sharp feature at low kinetic electron emission energies. The second attribute of a negative electron affinity at the surface is determined from the width of the spectrum. The width of the photoemission spectrum (W) can be related to the electron affinity (χ). The spectral width is obtained from a linear extrapolation of the emission onset edge to zero intensity at both the low kinetic energy cutoff and at the high kinetic energy end (reflecting the valence band maximum). The following relations apply for the two cases:

$$\begin{aligned} \chi &= h\nu - E_g - W \quad \text{for a positive electron affinity} \\ 0 &= h\nu - E_g - W \quad \text{for a negative electron affinity} \end{aligned} \tag{1}$$

where E_g is the bandgap and $h\nu$ is the excitation energy. We stress that the photoemission measurements cannot be used to determine the energy position of the electron affinity for the NEA surface. Careful measurements of the width of the spectra are helpful in distinguishing whether the effect is direct emission of the electrons from conduction band states or excitons are involved in the emission process. The effects of excitons have recently been reported by Pate and co-workers [4].

Field emission measurements were obtained in an ultra-high vacuum (UHV) system with pressures typically $< 1\times10^{-8}$ Torr. A cylinder of molybdenum (3mm diameter) was selected as the anode for these measurements. The end of the cylinder was either polished flat or polished to a very high radius of curvature (typically > 5mm) to minimize edge effects. The anode is mounted on a stage that is coupled to a UHV stepper motor. One step of the motor corresponds to movement of the anode by 0.055μm. Current-voltage measurements are acquired with a

computer controlled Keithley 237 Source Measure Unit (SMU). The SMU has the ability to simultaneously source a voltage and measure a current. A current limiting circuit is also included within the SMU so that no voltage is applied that causes the current to exceed 1×10^{-7}A.

In any given measurement, a family of I-V curves is recorded with each curve corresponding to a different anode to sample spacing. Initially, the anode is positioned at some unknown distance above the sample. The stepper motor count is recorded and an I-V curve is collected. Next, the anode is moved closer to the sample by a known distance, and the cycle is repeated until at least 5-10 curves are collected. As expected, the current-voltage curves shift to lower voltage values with decreasing distance. Because of the nature of the Fowler-Nordheim I-V equation, the "turn-on" voltage or threshold voltage must be defined in terms of a specific current value. The voltage that results in a current value of 10nA was chosen to represent the threshold voltage for electron emission. This value was chosen because it is two orders of magnitude above the inherent noise current in our system. Next, each threshold voltage is plotted versus distance relative to the first I-V curve, and as expected, the resulting graph was linear. Upon fitting the data to a straight line, the slope represents the average field for the threshold current emission. This method for determining the average field does not rely upon the absolute anode to sample spacing, but rather the change in distance of the anode with respect to the sample.

The PEEM measurements were obtained using a high resolution system from Elmitec. The sample holder supports a 5mm dia. substrate and employs electron beam assisted heating to greater than 1000 °C. The base pressure in the microscope is $\sim2\times10^{-10}$ Torr. The Elmitec system employs an electromagnetic immersion lens, and has a lateral resolution of 10 nm. The sample is held a potential of -20,000V while the electron column is at ground potential. The field is applied by an anode (ground) positioned 2 mm from the sample surface (average field of 10 V/μm). The electrons are focused onto a microchannel plate and phosphor, and the image is recorded with a CCD camera outside the vacuum. Most measurements were obtained with UV light from a 100 W Hg lamp focused onto the sample. The light is incident on the sample at an average angle of 16 degrees. The high energy cutoff of the Hg lamp is ~ 5.1 eV. In some instances the spontaneous radiation from a free electron laser system was employed to obtain images. The light was obtained from the OK-4 UV free electron laser at the Duke University Free Electron Laser Laboratory.

In all experiments, separate images were also obtained with the light turned off. In some cases weak images were visible induced by only the applied field. These images are termed field electron emission microscopy (FEEM) images.

Results and Discussion

Photoemission of Diamond and Nitrides. The electron affinity of a semiconductor has been discussed in the same terms as the work function of a metal. The work function of a perfect metal surface is ascribed to aspects related to the electronic levels of the atoms involved in the material and the surface dipole. In the most fundamental terms, the surface dipole of a metal is related to the fact that the electron wave function extends beyond the potential defined by the atomic core. The electron density at the surface is balanced by an electron deficient region which results in a dipole. The field due to this dipole results in a potential which confines electrons in the material. This is a very simplified picture; in practice, it is not possible to calculate the surface dipole term, but it is possible to discuss how changing the surface changes the surface dipole. In general terms, the adsorption of an atomic species that is more electronegative than the surface atoms will increase the electron affinity while adsorption of a more electropositive species will decrease the electron affinity.

For a semiconductor, the actual electron orbitals and bonding configuration will come to play in determining whether a change in the surface termination results in an increase or decrease in the electron affinity. For diamond it is recognized that oxygen termination of clean surfaces result in a positive electron affinity while hydrogen termination results in a negative electron affinity [3].

The results of an extensive UV photoemission study of surface preparation processes on type IIb diamond are summarized in Table 1 [5]. The initial diamond surfaces were prepared with either a chromic acid etch or an electrochemical etch in water. Both processes have been shown to result in oxygen termination, but it is evident (see Table 1) that the oxygen desorbs from the surfaces at slightly different temperatures for the different cleaning processes. There is a larger difference in the desorption temperature for the different surface orientations. For the (100) surface, oxygen is observed to completely desorb at ~900°C while for the (111) and (110) surfaces, the oxygen desorbs for annealing at 700°C or less. We note that the hydrogen termination on all three surfaces results in a NEA, and again the hydrogen termination is stable to higher temperatures on the (100) surface.

Since large crystals of the III-V nitrides are not currently available, measurements have been obtained from epitaxial films. Recent measurements of AlN thin films grown on SiC indicates a NEA [6] while a positive χ of 3.3 eV is measured for GaN on SiC [7]. The results for these and several alloy films are summarized in Fig. 1. The alloy concentration was deduced from cathodoluminescence measurements of the bandgap and the assumption of a linear relation between 3.4 eV for GaN and 6.2 eV for AlN. The results suggest that a negative electron affinity is obtained for these surfaces with AlN percentages of ~70% or greater. To date there have not been measurements of the effect of surface adsorbates, but a theoretical analysis indicates that molecular adsorbates such as hydrogen will behave differently on the different nitride surfaces [8].

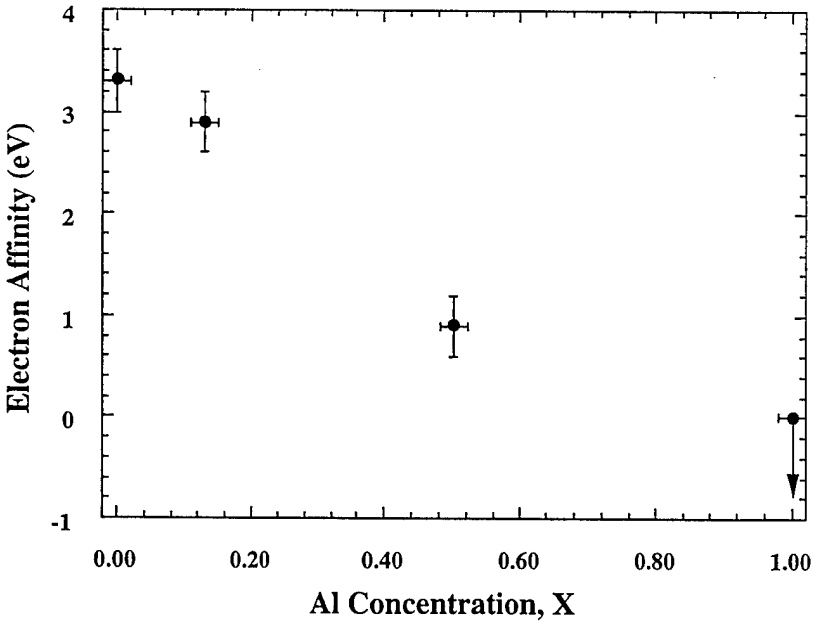

Figure 1. Plot of the electron affinity versus alloy concentration for AlGaN alloy films grown on 6H-SiC (0001). The values were deduced from UV photoemission, and we note that negative values cannot be obtained with this technique.

Field Emission - Moving Probe. Field emission properties were measured using a position variable anode system. This technique has the advantage that the dependence of the emission on the anode to cathode spacing can be measured. In addition, the technique is not as sensitive to parallelism of the anode and cathode surfaces which often presents problems when using a spacer apparatus to measure field emission properties. Also, obtaining the high vacuum required for electron emission is accomplished more easily with the position dependent anode system, and the system is not susceptible to breakdown of the dielectric spacer.

Field emission measurements were applied to the p-type natural diamonds after various surface treatments [5]. Type IIb diamond (100) and (110) samples were prepared with the electrochemical cleaning processes and then loaded into the UHV moving probe field emission system. A (110) sample was also exposed to a hydrogen plasma and transferred directly to the field emission system. Field emission measurements were obtained at several distances, and the distance was determined by relating the measurements to the point of contact. This process leads to some uncertainty, but for these conducting substrates, it is not a critical issue. The average threshold field for the measurements is shown in Table 1. Here, very high values were obtained from the oxygen terminated surfaces and a low value was obtained from the hydrogen terminated surface.

Table 1. Summary of the UPS and on C(100), (111) and (110) type IIb natural diamond surfaces. (RT: room temperature, χ: electron affinity, PEA: positive electron affinity, NEA: negative electron affinity) Unless noted otherwise the surfaces have been cleaned by an electrochemical etch. The experimental uncertainties are 0.1 eV. Also field emission results of C(100) and (110) and are shown.

Surface				
C(100) after chromic acid clean	500°C PEA, χ = 1.00 eV	900°C PEA, χ = 0.70 eV	1100°C NEA, χ < 0	
C(100) after electrochemical etch	PEA, χ = 1.45 eV	NEA, χ < 0	PEA, = 0.75 eV	
C(100) after electrochemical etch	900°C NEA, χ < 0	H-plasma NEA, χ < 0	1100°C PEA, = 0.75 eV	H-plasma NEA, χ < 0
C(111) after chromic acid clean or electrochemical etch	RT to 600°C NEA, χ < 0	H-plasma NEA, χ < 0	900°C PEA, χ = 0.5 eV	
C(110) after electrochemical etch	700°C NEA, χ < 0	800°C PEA, χ = 0.6 eV	H plasma NEA, χ < 0	800°C PEA, χ = 0.6 eV

	Field Emission threshold
C(100) after electrochemical etch	79 V/μm
C(110) after electrochemical etch	81 V/μm
C(110) after H plasma treatment	25 V/μm

While n-type diamond is not commonly available, single substitutional nitrogen doped diamond can be prepared with a deep donor 1.7 eV below the conduction band. Geis *et al.* [9] have suggested that a Schottky contact, which is formed when type Ib single crystal diamond is metallized with nickel, may be sufficient to supply electrons into the conduction band of the diamond. In this model, the applied voltage would be dropped primarily across the metal/diamond interface, and a low field at the NEA surface would result in emission into vacuum. Figure 2 shows the field emission properties of a nitrogen doped film grown with [N]/[C] = 0.2. The average threshold field (for 10 nA emission) for this sample was 64V/μm. After field emission measurements, damage to the diamond film and substrate was observed by optical microscopy. Micro-arcs between the sample and the anode are the most likely explanation for the observed damage [10]. These position dependent field emission measurements indicate that an injecting contact is not formed for these films. It is likely that the observed emission is directly from the Si substrate at the points of damage.

Field emission measurements have also been obtained from pyramid structures of Si doped GaN.[11] These structures are prepared by selective OMCVD growth processes [11]. We note that the surfaces were prepared with a hydrogen plasma exposure prior to the field emission measurements. This process was employed as an *in situ* cleaning process, and Auger electron spectroscopy verified removal of surface carbon contamination, but the treatment did not affect the monolayer surface oxide termination. The field emission results are presented in Fig. 3. This surface exhibits the lowest threshold of any sample that we have measured to date. Similar measurements from flat surfaces of similar films exhibit average threshold field of ~50 V/μm.

PEEM Imaging of III-V-Nitride and Diamond Films. The technique of PEEM and FEEM has previously been applied to the study of CVD diamond thin films. Wang *et al.* [12] have reported electron emission from CVD diamond films with field strengths as low as 3V/μm, and it was suggested that the emission is due to the negative electron affinity of the diamond surfaces. Shovlin and Kordesch [13] report inducing low field cold emission in a partially oriented ([100] texture) diamond film by depositing 7nm of gold on the surface. While most studies have employed a Hg lamp to excite the PEEM image, synchrotron PEEM was performed on diamond films and uniform emission was observed [14]. We report in Fig. 4 PEEM images comparing boron and nitrogen doped films. The images show emission from all surfaces with stronger emission from the edges near the surface. The differences in the images reflects the differences in the surface morphology as evidenced by SEM of the same samples. Raman analysis of these films shows a low concentration of sp^2 bonded carbon, and we do not detect enhanced emission from graphitic grain boundaries. The observed enhanced emission from the edges is likely due to field enhancement from the applied field of the

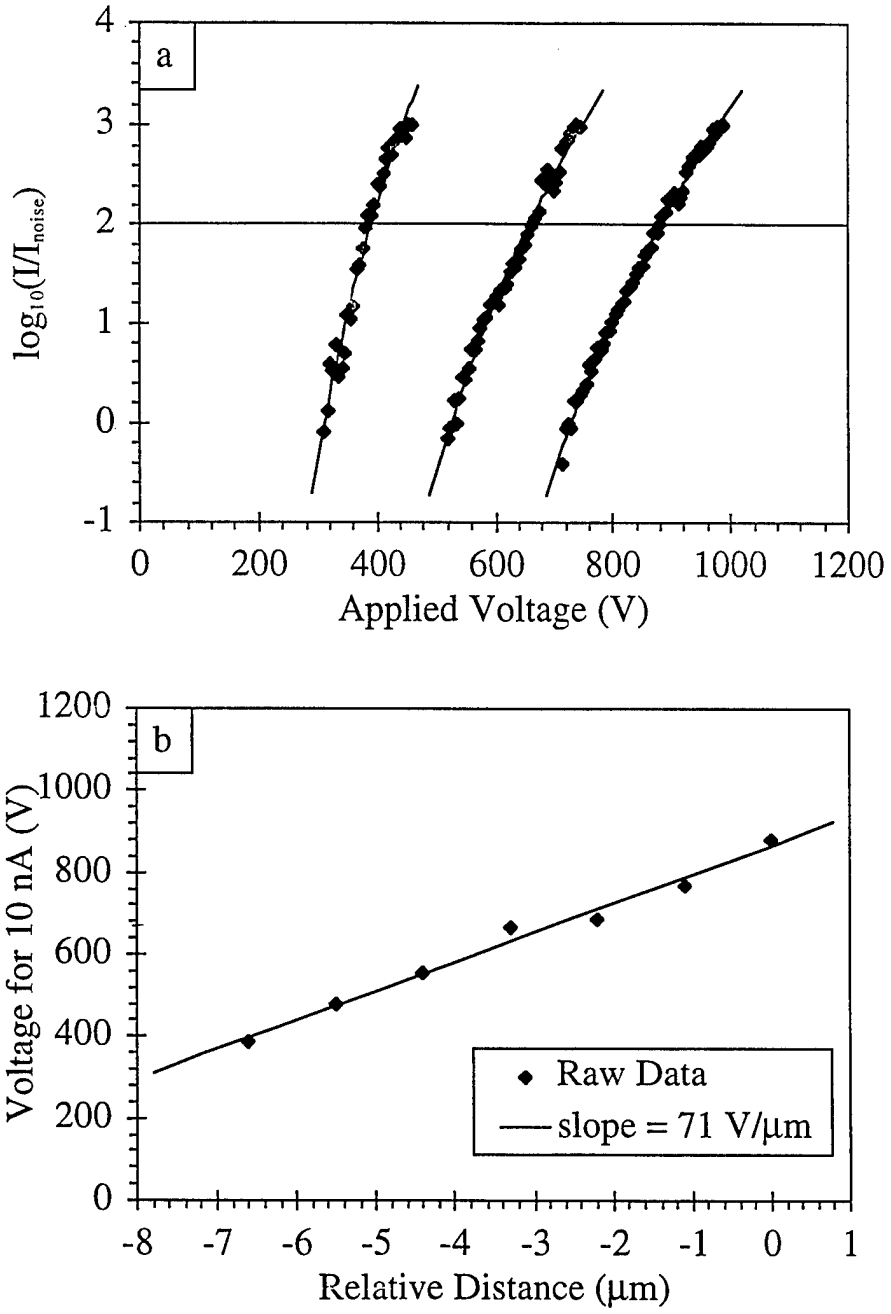

Figure 2. Field emission measurements of a nitrogen doped diamond film obtained at various anode to sample distances (a), and an analysis of the average field required to obtain an emission current of 10 nA (b). In (a) the current has been normalized by the background noise current and is plotted on a log scale (I_{noise} = 0.1 nA). The distance scale in (b) was measured relative to the first measurement position, and subsequent data were obtained as the anode was moved towards the surface. The slope of the plot in (b) is 71 V/μm.

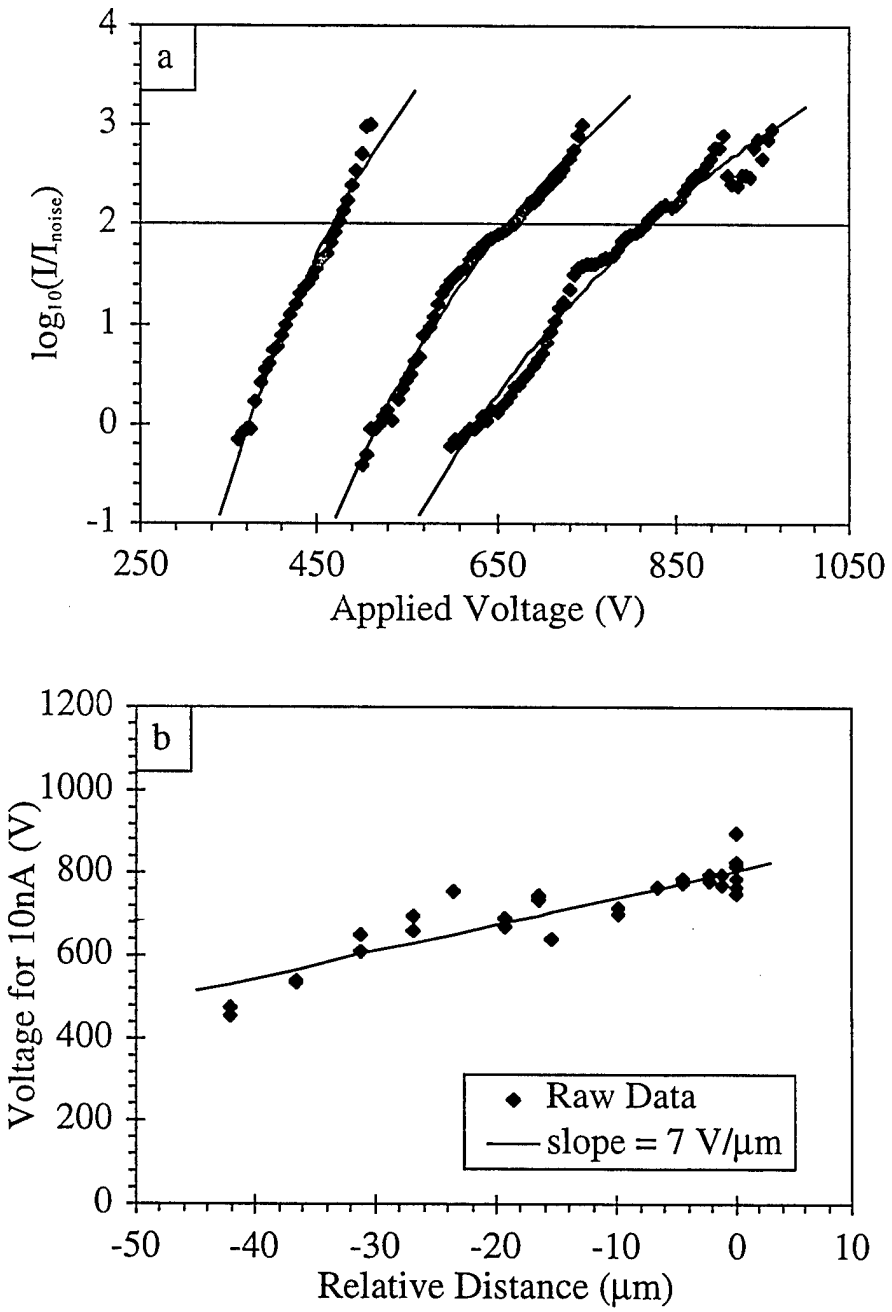

Figure 3. Field emission measurements of a Si doped GaN pyramid array. The measurements were obtained at various anode to sample distances (a), and an analysis of the average field required to obtain an emission current of 10 nA (b). The slope of the plot in (b) is 7 V/μm.

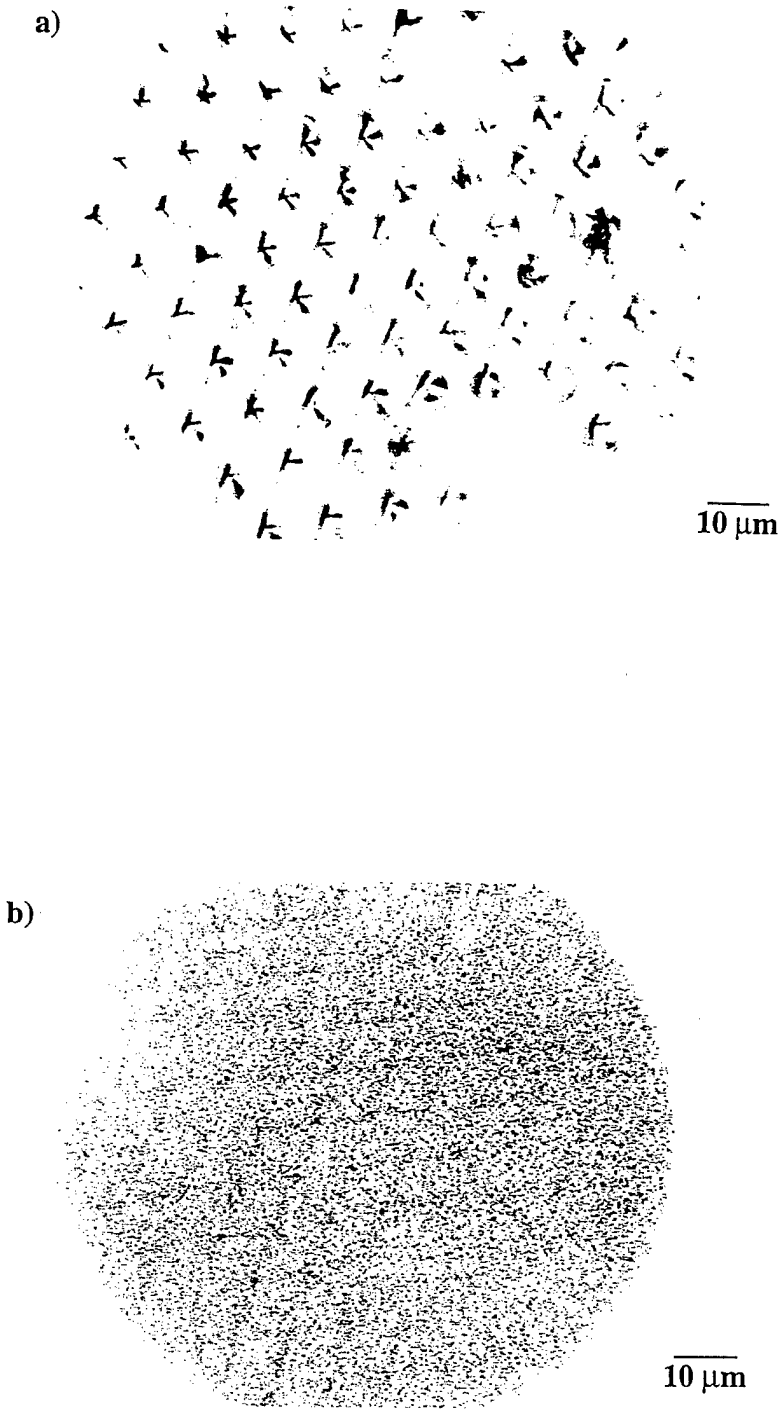

Figure 4. PEEM image of p-type diamond film (a) and a nitrogen doped film (b). In these images the dark regions represent the areas of intense electron emission. A 100W Hg lamp was used to obtain (a) while the spontaneous radiation from the UV FEL at Duke University was used to obtain (b).

microscope. For these samples, we were not able to detect FEEM images. This is consistent with our field emission measurements which showed threshold emission fields greater than the 10V/μm available in the microscope system.

The PEEM and FEEM images of the Si doped GaN pyramidal array are displayed in Fig. 5. Note that emission is observed from the regions near the peaks of the GaN pyramids, and that emission intensity is nearly uniform for each of the emitters over the array. Moreover, emission is observed in the FEEM image, and this is again consistent with our field emission measurements which showed an emission threshold less than 10 V/μm.

Concluding Remarks

The results presented here demonstrate the necessity for a series of complimentary measurements in order to characterize the properties of wide bandgap materials for electron emission applications. It is evident that the electron affinity is a critical limiting aspect for field emission from conducting p-type diamond and Si doped GaN. It appears that the electron emission from p-type diamond is from the valence band of the material, while evidence suggests that the field emission from Si-doped GaN originates from electrons in the conduction band. Moreover, we were not able to obtain emission from nitrogen doped diamond without damaging the surfaces. This suggests that the emission threshold is greater than the measured value of ~70V/μm. The high field required for emission from these samples seems inconsistent with the proposed model for the effect of single substitutional nitrogen. The PEEM measurements were fully consistent with the field emission measurements. In the PEEM from diamond, emission was observed from all surfaces with some enhancement at the edges. This was attributed to the field in the microscope.

The Si doped GaN pyramid structures displayed the lowest field emission threshold of our samples, and both PEEM and FEEM emission showed relatively uniform emission originating from the peaks of the structures.

Another technique that is critical for characterizing field emission materials is field emission energy distribution (FEED). In this technique, the energy spectrum of the emitted electrons is analyzed. This technique is important because the energy of the emitted electrons can be determined with respect to the contact Fermi level. This allows determination of whether the emission is from metallic states at the Fermi level or from the valence or conduction bands of a semiconductor.

The results for the diamond-type material systems described here show promise for the development of cold cathode emitters. While relatively low field emission thresholds have been reported for p-type diamond, the development of n-type doping could certainly improve the performance of diamond based emitters. For the nitrides, it appears that n-type GaN holds real

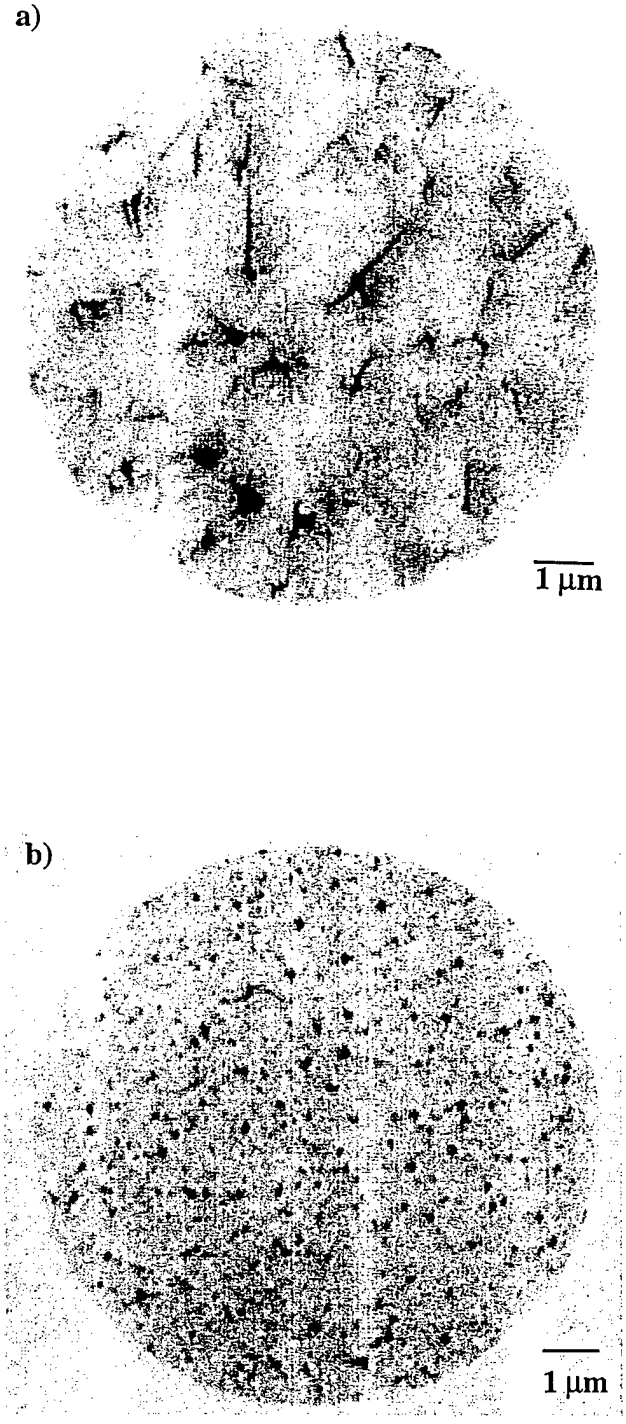

Figure 5. PEEM image of the pyramid structures of the Si doped GaN (a), and FEEM image of the same surface (b). In these images the dark regions represent the areas of intense electron emission. The images were excited with a 100 W Hg lamp.

promise as an electron emitter. The development of selective growth processes to produce pyramid structures which combine the low work function and field enhancement is one approach. Another will be to explore AlGaN alloys with increased Al concentration while still maintaining n-type doping. To date n-type character has been reported for AlGaN alloys with ~40% AlN, and theoretical analysis suggests that doping of alloys with up to 60% AlN is possible. There have been no reports to date on the effects of different surface terminations of the nitrides, while it is now established that surface termination strongly affects the emission character of diamond surfaces. Future research is in progress to address these issues.

Acknowledgments

We gratefully acknowledge H. Ade for discussions on the PEEM measurements, and we are very appreciative of O.K. Nam and R.F. Davis for supplying the nitride samples employed here and in our previous studies. We also acknowledge the Duke University FEL Laboratory for access to the OK-4 UV FEL. This project was supported through the Office of Naval Research.

References

1. F.J. Himpsel, J.A. Knapp, J.A. van Vechten, D.E. Eastman, Phys. Rev. B **20**, 624 (1979).
2. B.B. Pate, Surf. Sci. 165, 83 (1986).
3. J. van der Weide and R.J. Nemanich, Phys. Rev. B, **49** (1994) 13629.
4. C. Bandis, and B.B. Pate, Phys. Rev. Lett. **74**, 777 (1995).
5. P.K. Baumann and R.J. Nemanich, Surface Science, (in press).
6. M. C. Benjamin, C. Wang, R. F. Davis, and R. J. Nemanich, Appl. Phys. Lett. **64**, 3288 (1994).
7. M.C. Benjamin, M.D. Bremser, T.W. Weeks, Jr., S.W. King, R.F. Davis, and R.J. Nemanich. Applied Surface Science **104/105**, 455 (1996)
8. R.J. Nemanich, M.C. Benjamin, S.W. King, M.D. Bremser, R.F. Davis, B. Chen, Z. Zhang, and J. Bernholc. *Gallium Nitride and Related Materials*, edited by F.A. Ponce, R.D. Dupuis, S. Nakamura and J.A. Edmond. (Mater. Res. Soc. Symp. Proc. vol **395,** 1995) pp 777-788.
9. M.W. Geis, J.C. Twichell, J. Macaulay, and K. Okano, Appl. Phys. Lett. **67**, 1328 (1995).
10. O.M. Kuttel, O Groning, E. Schaller, L. Diedrich, P. Groning and L. Schlapbach, Diamond and Related Mater. **5**, 807 (1996).
11. O.-H. Nam, M.D. Bremser, B.L. Ward, R.J. Nemanich, and R.F. Davis, Jpn. J. Appl. Phys. **36**, L532 (1997).
12. C. Wang A. Garcia D.C. Ingram M. Lake, M.E. Kordesch, Electronic Lett. 27, 1459 (199?)
13. J.D. Shovlin, M.E. Kordesch, Appl. Phys. Letters **65**, 863 (1994)
14. J.D. Shovlin, M.E. Kordesch, D. Dunham, B.P. Toner, W. Engel, J. Vac. Sci. Technol. A **13**, 1111 (1995).

III. Fabrication and Testing of a Diamond Microstrip Particle Detector

S. K. Han, M. T. McClure, C. A. Wolden*, B. Vlahovic**, A. Soldi**, Z. Sitar
Materials Science and Engineering, North Carolina State University, Raleigh, NC
**presently at Colorado School of Mines, Golden, CO*
***North Carolina Central University, Durham, NC*

A particle detector for high flux applications has been fabricated based on highly oriented diamond (HOD) films. Relatively thick HOD films were achieved by combining the bias enhanced nucleation (BEN) in a microwave plasma chemical vapor deposition (MPCVD) reactor and high rate growth process in a low pressure combustion flame (LPCF) reactor. Following the diamond deposition, Si substrate was etched away to obtain a free standing, 4 mm diameter diamond membrane. A Ti/Au microstrip electrode pattern was applied to one side of the detector to provide spatial resolution. The detector performance was tested by measuring energy spectra of α-particles emitted from an ^{241}Am source. As compared to the performance of a polycrystalline diamond detector, the HOD detector showed a three to four fold improvement in performance, which was close to that obtained for single crystalline diamond detectors.

Presented to J. Applied Physics

A. Introduction

Since conventional Si detectors can easily be destroyed in high energy high flux environments, detectors based on more robust materials are desired. In addition to radiation hardness, an ideal material should posses a high thermal conductivity, high breakdown voltage, and a high melting point. Diamond is an ideal candidate for such detectors since it unites all the required properties [1,2]. It has a thermal conductivity 4 times greater than Cu, a breakdown voltage of 10^{11} V/cm, a high radiation hardness, and is stable at temperatures in excess of 1000°C. As such, a diamond detector can be exposed directly to a high intensity beam without suffering significant thermal or radiation damage. Due to its high electrical resistivity, high electric fields can be applied across the detector without significant increase in the leakage current. In addition, a simple metal-diamond-metal (m-d-m) structure can be used as a detector element, instead of a reverse pn junction diode used in conventional Si-based detectors. Table I summarizes diamond properties relevant for detector application and compares them with those of Si.

For the best performance of such an m-d-m device, single crystalline diamond is desired; however, it is prohibitively expensive for large area applications. An economically viable alternative to the single crystals are CVD diamond films. Unfortunately, the grain boundaries in randomly oriented CVD diamond films act as transport barriers, leakage paths, and considerably reduce the thermal conductivity. This all makes the detectors based on polycrystalline films inferior to those fabricated from single crystalline material. In addition to randomly oriented CVD films, there has been significant progress also on highly oriented diamond (HOD) films [3-5] which exhibit almost single crystalline properties in the growth direction. Since the signal in an m-d-m detector is collected uniaxially, single crystallinity can be mimicked in the charge collection direction by producing HOD films. Such films can be grown on silicon by coupling of bias enhanced nucleation (BEN) and van der Drift "evolutionary selection growth" process [6,7].

For the success of this process, a high nucleation density and a high degree of orientation of initial nuclei is mandatory. The BEN procedure developed for MPCVD [7] produces a nucleation density of about 10^{10}/cm and, at proper process parameters, also a high fraction of oriented nuclei (30-50%). If, following the nucleation, the growth parameters are such that the (100) oriented nuclei have their fastest growth direction perpendicular to the substrate, they will overgrow all randomly oriented nuclei and survive at the surface, resulting in a (100) oriented film, as shown in Fig. 1. Once the misaligned grains are eliminated from the growth surface, significant grain boundary reduction (or even elimination) is possible as adjacent oriented crystals coalesce.

Although the MPCVD process is capable of producing HOD films, the achieved maximum growth rates in a 1 kW reactor are rather low (on the order of 0.1 μm/hr). Our previous

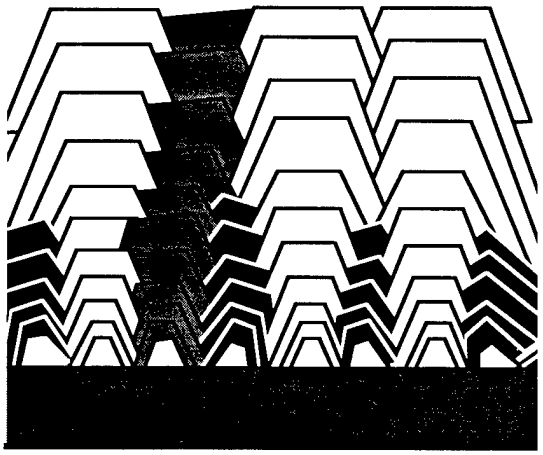

Figure 1. Schematic representation of the "evolutionary selection growth" process.

experiments in a low pressure combustion flame (LPCF) reactor have demonstrated that the preferential growth of (100) oriented particles can be controlled at up to 50 times higher growth rates than those achieved in MPCVD reactors [8]. Since the LPCF process does not provide a possibility for the control of nucleation, thick, HOD films can be produced by combining MPCVD and LPCF technique [9]. By combining the two techniques, the processing time is reduced significantly due to inherent high growth rates in an LPCF system.

This paper describes in detail the processing steps applied in the fabrication of the particle detector, as well as gives the results on test measurements and compares them to those obtained from a detector based on randomly oriented diamond.

B. Detector Fabrication

Single crystal, (100) oriented Si wafers were used as substrates. Prior to deposition, they were cleaned consecutively with acetone, methanol, and isopropanol and finally etched in a diluted HF solution. In the MPCVD system, the substrates went through a four step deposition process consisting of a hydrogen plasma clean, surface carburization, BEN, and diamond growth. Hydrogen plasma cleaning was performed to remove any atmospheric contamination that occurred during the loading of the substrates into the deposition system. During the carburization step, the substrate surface was saturated with carbon at a high temperature (900°C) in a methane/hydrogen plasma. A negative DC bias of 210 V was applied to the substrate during the BEN process in order to attract and energize positive carbon ions. At the end of this step, the bias voltage was turn off and the system parameters were changed to the appropriate conditions for oriented growth. The films were grown in the MPCVD reactor until a thickness of about 1 μm was reached. Sample were then transferred to the LPCF reactor for the final growth step. In the LPCF system, C_2H_2/O_2 flame was used to further grow HOD to a thickness of 15 μm. The deposition temperature was 760°C as measured by an optical pyrometer. Table II summarizes the process parameters for each deposition step.

Figure 2(a,b) shows the resulting surface morphologies after the MPCVD and LPCF growth steps, respectively. As seen in Fig. 2(a), MPCVD resulted in well faceted diamond particles of up to 1 μm in size. Approximately 40% of the particles exhibited a (100) texture and were also azimuthally oriented with respect to each other. After deposition in the LPCF reactor, most of the "misaligned" grains were overgrown and highly oriented, 15 μm thick diamond films were produced, as seen in Fig. 2(b). Form the size of the newly developed grains, it is apparent that the neighboring crystallites have coalesced to form large area and high quality single crystalline diamond grains. In addition, the resulting films were relatively smooth and did not require any polishing before the device fabrication.

The device fabrication consisted of two distinct process steps: fabrication of a free standing diamond membrane and application of the top and bottom contacts. The main processing steps are schematically shown in Fig. 3.

Following the diamond deposition, wafers were coated with a layer of photoresist (PR). One cm long and 100 μm wide openings with a center to center spacing of 200 μm were patterned into PR to expose diamond for the deposition of contacts. Contacts consisted of a 200 Å thick layer of Ti and a 2000 Å thick layer of Au. A Ti interlayer was used to improve adhesion of gold and to form an ohmic contact with the diamond film [10,11]. Final definition of the top electrodes was achieved by a PR lift-off technique. An SEM image of the patterned top surface is shown in Fig. 4(a).

After the patterning of the top electrodes, Si substrate was removed from the back side to from a free standing diamond membrane. Most of Si was removed mechanically by dimpling; the process was finished with a preferential etch in a concentrated KOH solution. During the chemical etch step, the top surface with microstrip electrodes was protected by a layer of a chemically resistant wax. Figure 4(b) shows a completed, 4 mm diameter diamond membrane from the back side of the wafer before the application of the back contact. The same electrode metals an thickness as for the top electrodes were used also on the back of the membrane. The completed device was annealed at 500°C for 30 minutes to improve the contact between the Ti interlayer and diamond.

C. Detector Performance

Preliminary testing of the fabricated detector was performed by measuring the energy spectra of α particles from an ^{241}Am source with a characteristic energy of 5.5MeV. During the measurements, the detector was placed 1 cm from the source. The electron-hole pairs generated by the α particles inside the diamond membrane were separated by an applied bias of 20 V, creating a pulse signal proportional to the total number of collected carriers. This signal was amplified by a charge sensitive amplifier (AmpTek A250) and recorded by a data

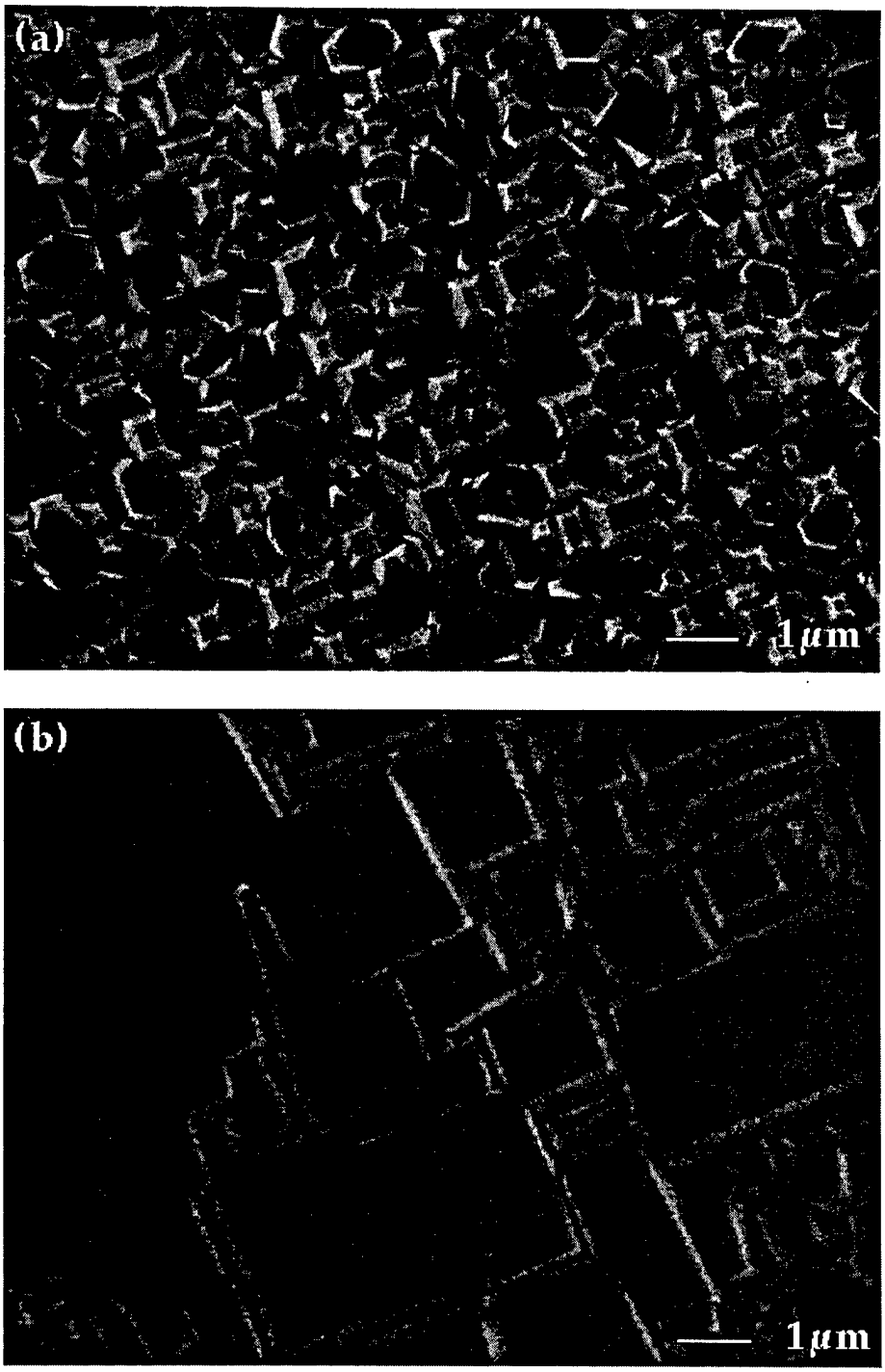

Figure 2. Surface morphology of (a) MPCVD grown and (b) LPCF grown diamond films.

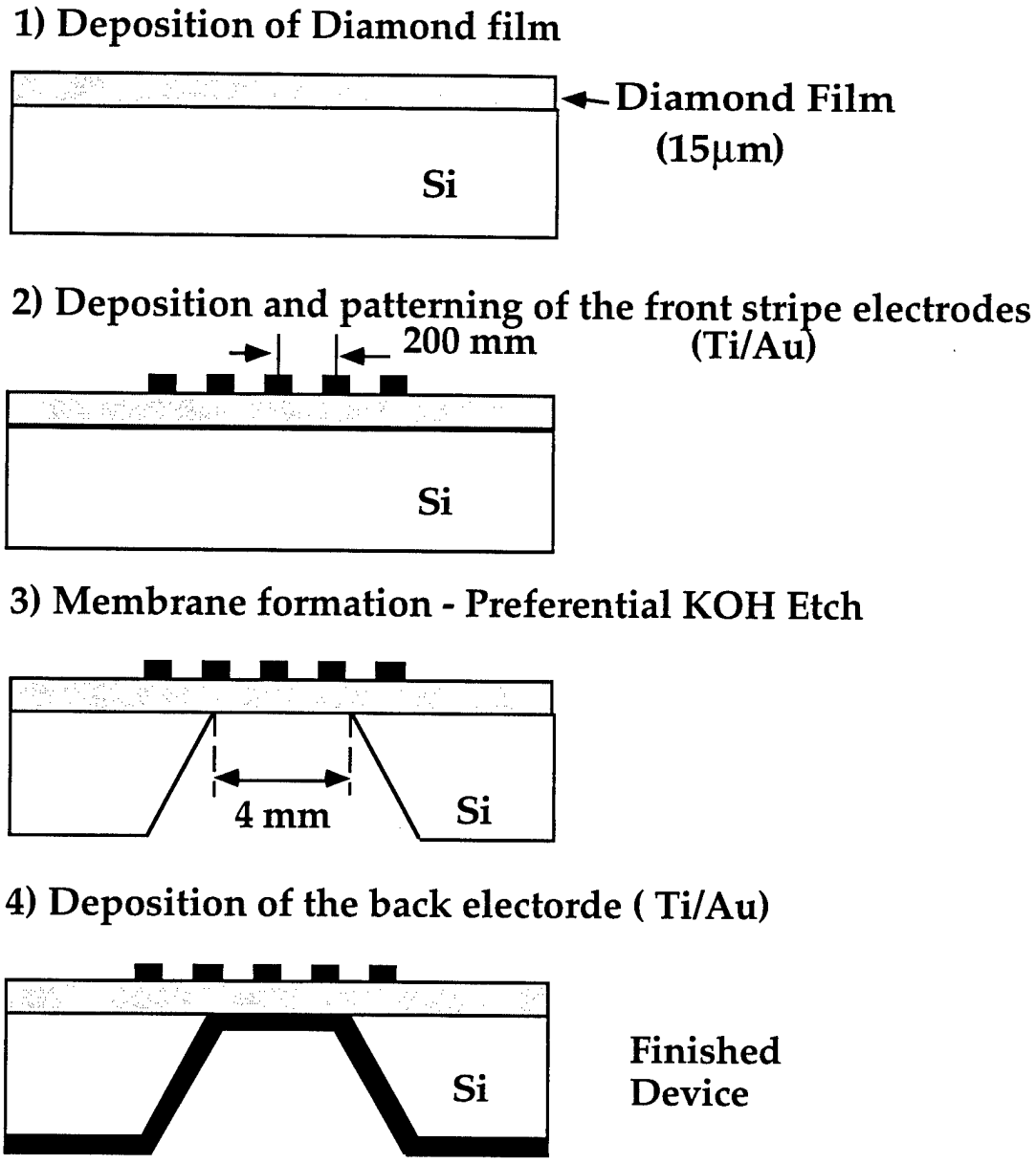

Figure 3. Main processing steps used in the fabrication of the detector.

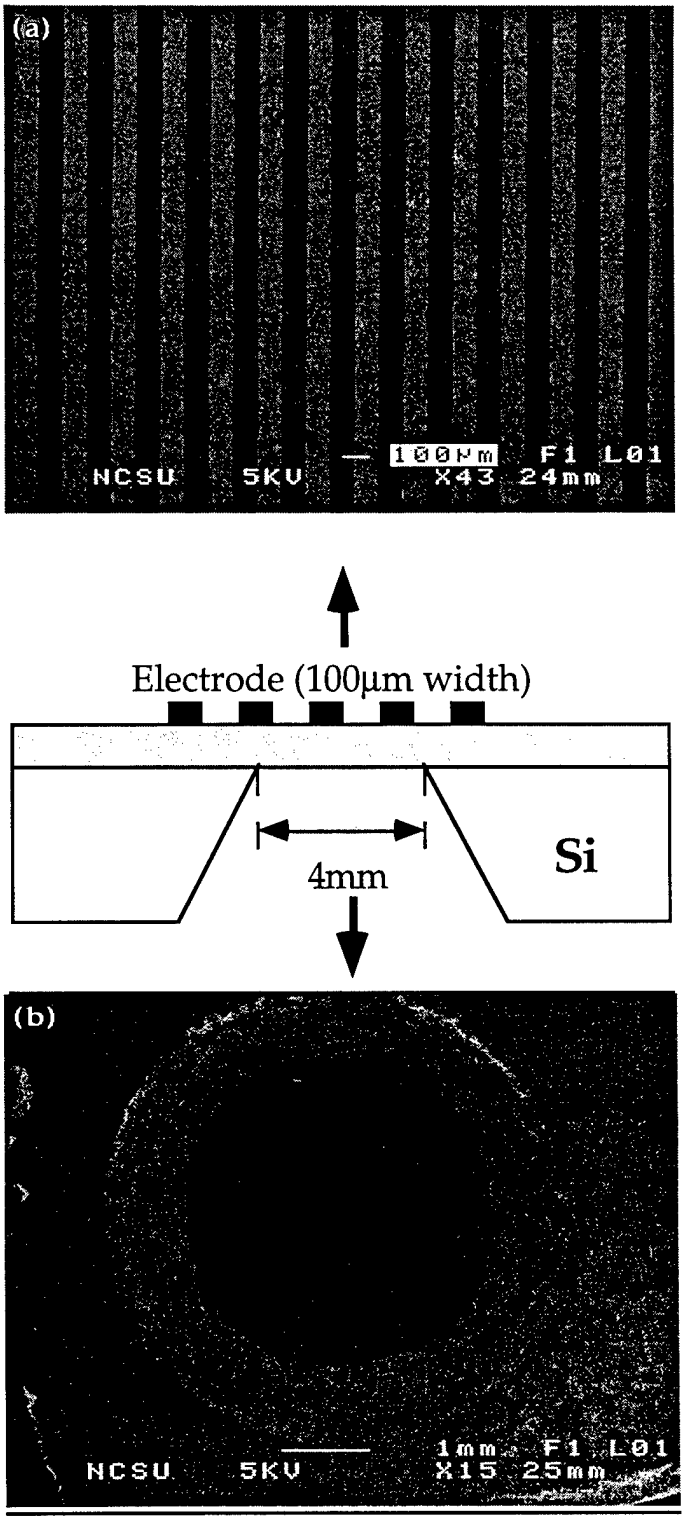

Figure 4. (a) Microstrip contact patterned on the top of the HOD films; (b) diamond membrane as seen from the back of the water.

acquisition system. The whole measurement setup was calibrated by discharging a reference capacitor. A schematic of the experimental geometry is shown in Fig. 5.

The measured α particle spectrum and a pulse obtained from a single α particle are shown in Figs. 6 and 7. Both figures show a high signal to noise ratio; in Fig. 6, the pedestal is well separated from the α particle spectrum and in Fig. 7 the height of the pulse is well above the signal threshold.

Since the total collected charge is proportional to the average distance traveled by the charge carriers before they recombine or are absorbed by the traps or impurities, the collection efficiency, C.E., can be estimated by the Hecht relationship [12]:

$$C.E. = \frac{Q_{collected}}{Q_{ionized}} = \frac{d}{w}\left(1 - e^{-\frac{w}{d}}\right),$$

where w is the thickness of the membrane and the collection distance, d, is defined as

$$d = \mu E \tau,$$

here μ represents the mobility, τ carrier lifetime, and E applied electric field.

Collection distance strongly depends on the quality of active diamond layer. Normally, values for state of the art detectors based on polycrystalline diamond range from 50 to 100 μm. In our case, we found the collection distances to be around 150 μm. This higher value can be explained by the high quality of HOD films, which have electrical properties superior to those of randomly oriented polycrystalline diamond.

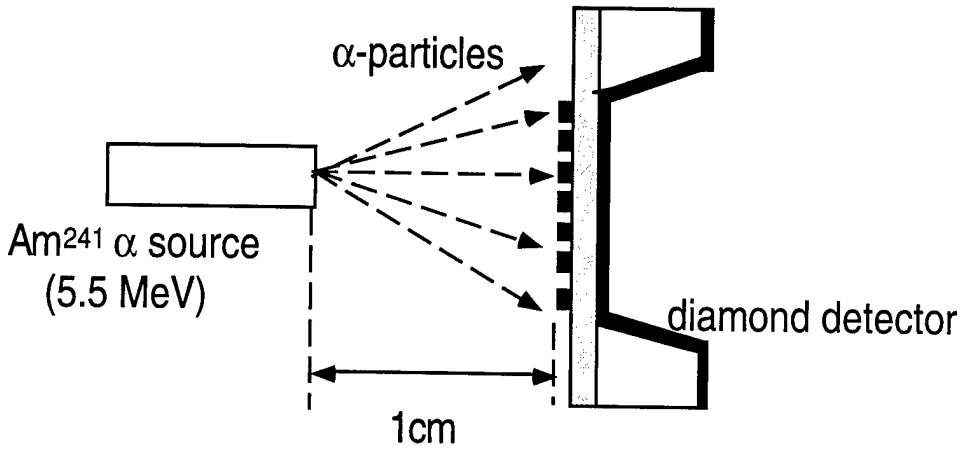

Figure 5. Schematic illustration of diamond particle detector and the testing arrangement.

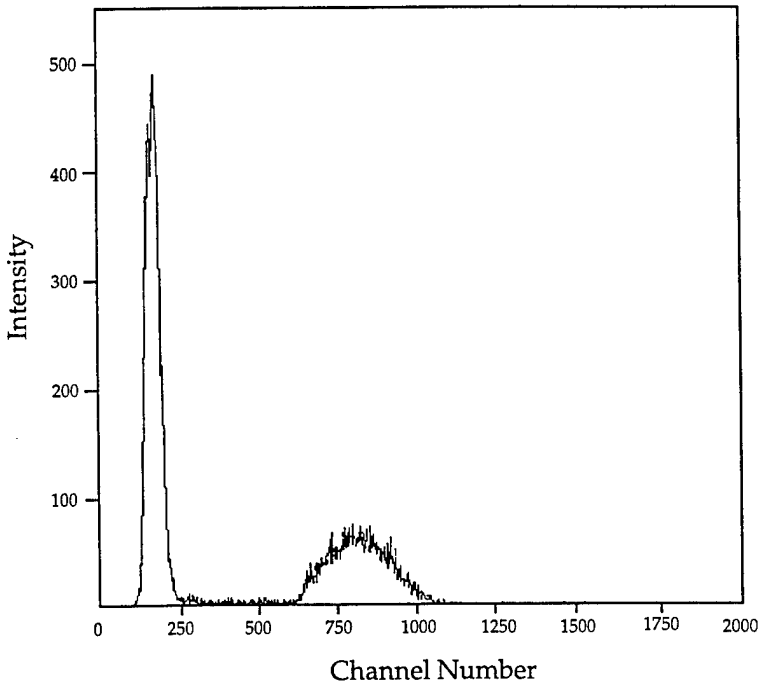

Figure 6. The pedestal and an alpha energy spectrum from ^{241}Am α source as detected by a detector based on HOD.

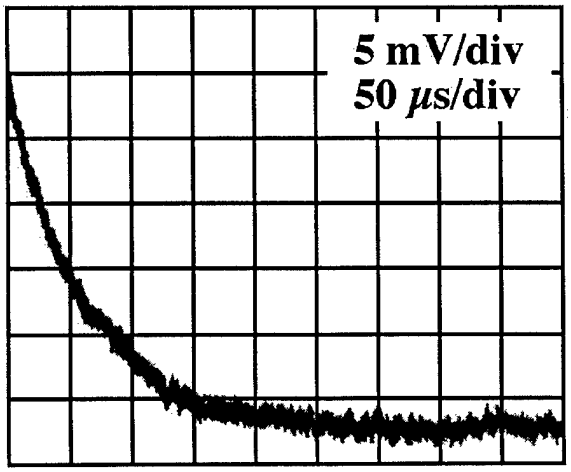

Figure 7. The pulse shape of a 5 MeVα particle on the same detector. The long decay time is related to the decay time of the charge sensitive amplifier, which is approximately 300 μs.

D. Conclusions

A diamond microstrip particle detector based on HOD films has been fabricated and tested. Thick HOD films were grown by coupling of BEN in a MPCVD system and oriented growth in a LPCF system. Following the diamond deposition, Si substrate was removed to form a free standing diamond membrane. Microstrip electrodes were pattern to measure the energy spectra and position of the incoming particles. As compared to the detectors based on randomly oriented diamond films, HOD detector showed a substantial improvement in the signal to noise characteristic and charge collection efficiency.

E. Acknowledgments

This work was supported by the Office of Naval Research under the grant #N00014-93-I-0437 and managed by Drs. M. Yoder and C. Wood.

F. References

1. M. Franklin, A. Fry, K. K. Gan, S. Han, H. Kagan, S. Kanda, D. Kania, R. Kass, S. K. Kim, R. Malchow, F. Morrow, S. Olsen, W. F. Palmer, L. S. Pan, F. Sannes, S. Schnetzer, R. Stone, Y. Sugimoto, G. B. Thmoson, C. White and S. Zhao, Nucl. Instr. and Meth. A **315**, 39 (1993).
2. H. Kangan, K.K. Gan, R. Kass, R. Malchow, F. Morrow, W.F. Palmer, C. White, S. Zhao, S. Schnetzer, M. H. Lee, S. K. Kim, F. Sannes, R. Stone, G. Thomson, D. Kania, S. Han, L. S. Pan, Y. Sugimoto, A. Fry, S. kanda, S. Olsen, M. Franklin, J. Angue, S. M. Ma, J. W. Ager, R. Wagner., 2nd International Conference on the Application of Diamond Films and Related Materials, p.29 (1993).
3. C. Wild, P. Koidl, W. Muller-Sebert, H. Walcher, R. Kohl, N. Herres and R. Locher, Diamond Rel. Mat. **2**, 158 (1993).
4. C. Wild, R. Kohl, N. Herres, W. Muller-Severt and P. Kohl, Diamond Rel. Mat. **3**, 373 (1994).
5. B. A. Fox, B. R. Stoner, D. M. Malta, P. J Ellis, R. C. Glass and F. R. Sivazlian, Diamond Rel. Mat. **3**, 382 (1994).
6. A. van der Drift, Phillips Res. Rep. **22**, 267 (1967).
7. S. D. Walter, B. R. Stoner, J. T. Glass, P. J. Ellis, D. S. Buhaenko, C. E. Jenkins and P. Southworth, Appl. Phys. Letts. **62**, 1215 (1993).
8. C. A. Wolden, Z. Sitar, R. F. Davis and J. F. Prater, Appl. Phys. Letts. **69**, 2258 (1996).
9. C. A. Wolden, S. K. Han, M. T. McClure, Z. Sitar and J. F. Prater, Mat. Lett. **32**, .9 (1997).
10. T. Tachibana, B. E. Williams, and J. T. Glass, Phys. Rev. B **45**, .975 (1992).
11. H. Shiomi, H. Nakahata, T. Imai, Y. Nishibayashi, and N. Fujimori, Jpn. J. Appl. Phys. **28**, 758 (1989).
12. J.W. Mayer, J. Appl. Phys. **38**, 296 (1962).

IV. Field Emission Energy Distribution Analysis of c-BN-Coated Mo Emitters: Nonlinear Behavior

B.L. McCarson, R. Schlesser, and Z. Sitar
Department of Materials Science and Engineering, North Carolina State University, Raleigh, North Carolina 27695-7919

Voltage-dependent field emission energy distribution (V-FEED) and current versus voltage (I-V) measurements were performed on Mo tips coated with intrinsic cubic boron nitride (c-BN) to determine the origin of the field-emitted electrons. Spectra were collected from the Mo emitters under ultra-high vacuum (UHV) conditions both before and after being coated. In some instances multiple FEED peaks were observed in the collected spectra. These corresponded to multiple emission sites on the emitter. The energy of the field-emitted electrons from the c-BN-coated emitters usually depended linearly upon the applied voltage and could be explained using a simplified band-bending model. However, at higher voltages the FEED measured from the c-BN-coated emitters departed from this linear behavior. These nonlinearities were attributed to a contact resistance at the Mo/c-BN interface which had a greater influence on the energy distribution of emitted electrons at larger emission currents.

A. Introduction

Research on the use of molybdenum as a field emitter for applications such as flat-panel display devices has yielded promising results [1]. However, the performance and stability of Mo emitters must be enhanced to meet the requirements of some applications [2,3]. This has prompted an interest in coating emitters with a chemically and mechanically stable material with superior emission properties. Tip-shaped Mo emitters which have been coated with wide band-gap materials have demonstrated enhanced emission properties relative to uncoated Mo emitters [4,5,6]. One such coating material is cubic boron nitride (c-BN). Not only is c-BN chemically inert and mechanically stable, but UV-photoemission studies have shown that c-BN features negative electron affinity [7]. Additionally, field emission studies on flat n-type c-BN have shown that considerable emission currents are attainable [8]. However, the mechanisms responsible for field emission in these devices are not yet completely understood. Previous voltage-dependent field emission energy distribution (V-FEED) and current versus voltage (*I-V*) analyses have provided insight into the emission process, which has been described within the framework of a simplified band-bending model [9]. A linear shift in the energy of field-emitted electrons that was observed from well annealed samples was due to field-induced band-bending caused by a voltage drop across the dielectric coating material. However, a nonlinear behavior of emission energy has been observed at higher voltages. This paper addresses these additional effects whose explanation is beyond the scope of the linear model and provides a discussion of the methods used for testing both bare and c-BN-coated Mo tips.

B. Methods

The Mo emitters used in this study were fabricated by electrochemically etching a 125 μm diameter Mo wire to a tip-like morphology. During the etching process, the Mo wire was biased at +10 V DC and submerged in a concentrated potassium hydroxide solution with a platinum counterelectrode. Scanning electron microscopy (SEM) was used to monitor the tip radii of curvature. Typical radii were less than 100 nm. The Mo tips were then coated with nominally intrinsic c-BN by an electrophoretic procedure where the Mo tips were submerged in an ultrasonically prepared suspension of c-BN particles in ethanol and again biased at +10 V DC (also with a platinum counter electrode). Typical c-BN particle size was approximately 100 nm. The uniformity and thickness of the c-BN coating were monitored by SEM. Coatings were usually a few hundred nanometers thick.

For the FEED and *I-V* analysis, the coated and bare emitters were secured in a holder so that each tip was centered 500 μm beneath a metallic gate with a 500 μm circular opening. The holder and tip were then placed in a UHV analysis chamber with a base pressure of 10^{-9} Torr where they were thermally annealed at 500°C for several hours. The holder was then aligned with the entrance lens of a hemispherical electron analyzer (VG Instruments, CLAM II). The

electron analyzer recorded the energy distribution of the field-emitted electrons which passed through the opening of the gate. Both the gate and analyzer were at ground potential while the emitter was biased negatively using a high voltage source with an integrated picoammeter (Keithley 237). The energy of field-emitted electrons was referenced to the Fermi level (E_F) of Mo using the following relationship [6]:

$$(E - E_F) = E_{kin} - eV + \Phi_A, \quad (1)$$

where V represents the potential applied between the gate and the tip, e the elementary charge, and E_{kin} the measured kinetic energy of field-emitted electrons. The analyzer work function, $\Phi_A = 4.3$ eV, was calibrated using a method described elsewhere [5]. All measurements were performed at room temperature.

C. Results and Discussion

The field emission current and energy distribution of the electrons emitted from bare Mo and the c-BN-coated Mo tips were collected at varying applied voltages. As described elsewhere, the energy ($E - E_F$) of the electrons emitted from bare Mo was well defined and did not depend upon the potential applied between the tip and gate [5,6]. The energy ($E - E_F$) of the electrons emitted from the c-BN-coated tips usually decreased monotonically with the applied voltage. This difference in behavior between emission from c-BN and Mo is best illustrated in Fig. 1. An emitter that was only partially coated with c-BN emitted at two different kinetic energies, thus leading to two distinct peaks in the FEED spectra. The position of one energy peak was dependent upon the applied voltage and represented field emission from a region of the tip that was coated with c-BN. The position of the other energy peak was not voltage dependent and represented emission from a region of the tip where the Mo was exposed. The position of the Mo peak provided an energy reference for the definition of E_F, independent from spectrometer calibration for the energies of the electrons emitted from the c-BN emission site.

In Fig. 2, a different emitter, which was completely coated with c-BN, displayed two voltage-dependent energy peaks. In this scenario, two emission sites on the same emitter were active while the spectra were recorded. However, the two emission sites were from different areas on the c-BN coating which did not have the same coating thickness. The two peaks shifted in energy by a different amount because the voltage drop across the dielectric depends upon the coating thickness. All the peaks displayed approximately linear shifts to lower energy with increasing applied voltage. Emission from the lower intensity site was less stable than the emission from the dominant site and would occasionally stop emitting altogether without any change to the applied voltage.

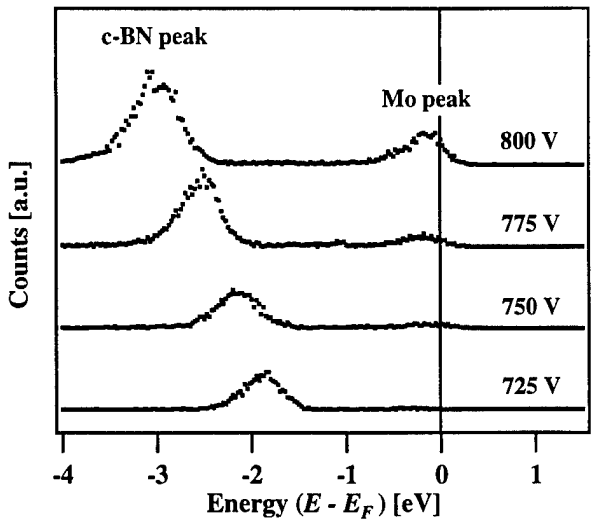

Figure 1. FEED spectra of a Mo emitter only partially coated with c-BN collected at different applied voltages. The position of one FEED peak was not voltage-dependent and represented emission from Mo. The position of the second peak was voltage-dependent and represented emission from c-BN.

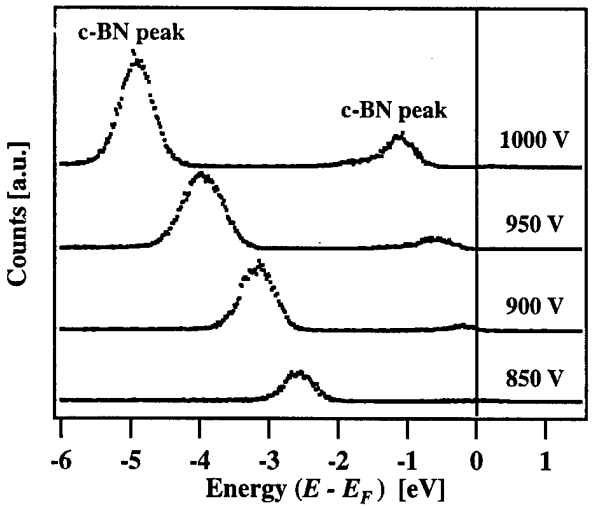

Figure 2. FEED spectra of a Mo emitter completely coated collected at different applied voltages. The positions of both FEED peaks are voltage-dependent and represent two different emission sites on the same emitter.

The linear shift in position of the c-BN energy peaks has been explained using a simplified band-bending model [9]. In this model, the change in energy is due to field-induced band-bending caused by a voltage drop across the dielectric c-BN coating. This voltage drop is proportional to the applied voltage and the thickness of the layer, and inversely proportional to

the dielectric constant of c-BN. Extrapolation of the peak position data from the linear region in Fig. 3 to flat-band condition yielded an intercept of 3.4 eV. Neglecting interfacial band-bending, this indicated that the field-emitted electrons originated 3.4 eV above the Fermi level of c-BN. The nominally intrinsic c-BN powder has a bandgap of 6.2 eV, [8] thus the observed emission probably originated from the conduction band minimum (CBM). Electrons are injected from the Fermi level of Mo into the conduction band of c-BN where they thermalize to the conduction band minimum and are then emitted from the c-BN/vacuum interface.

At higher applied voltages, the shift in position of the c-BN energy peaks were not always linear. Specifically, in Fig. 3 the position of the FEED peak shifted monotonically to lower energies with increasing applied voltage only until around 625 V. At voltages higher than 625 V, the peak shifted at a much higher rate. This behavior cannot be explained using the simplified band-bending model described above. Rather, an additional effect is needed to explain the total shift in the position of the FEED peak. A possible explanation would be that the total shift is due not only to the voltage drop across the c-BN coating, but also to an additional voltage drop due to a contact resistance across the Mo/c-BN interface. This anomalous shift in peak position has not been observed in diamond-coated Mo tips [4,5,6]. Thermal annealing of the diamond coated tips produced a conductive carbide layer between the diamond and the Mo [10]. A similar conductive layer could not be formed between c-BN and Mo through annealing.

The Mo/c-BN interface contact resistance can be estimated in the following way. Figure 4 is a Fowler-Nordheim plot of the current and voltage data collected from the sample described in Fig. 3. The dashed line represents an extrapolation of low-voltage data in a region of higher voltages, where nonlinear FEED peak shifts were observed. Figure 5 is a plot of measured

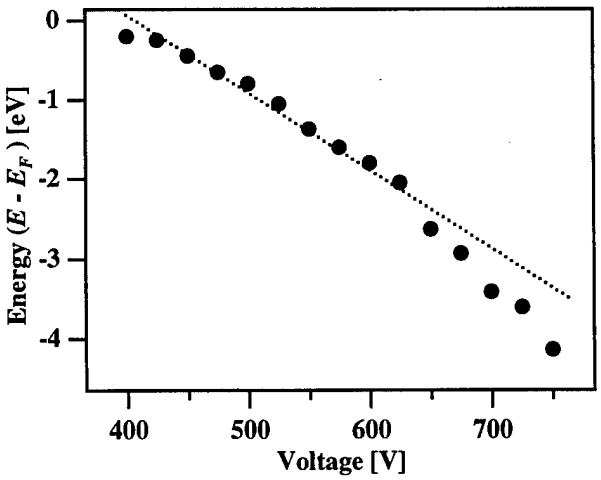

Figure 3. Shift in FEED peak position as a function of the applied voltage.

current versus FEED peak shift as a function of applied voltage (see also Fig. 3). In addition, the dotted line in Fig. 5 shows current data derived from the extrapolation of fitted F-N data shown in Fig. 4. The current from an ideal F-N emitter should increase exponentially with increasing voltage as can be seen in Fig. 5. The change in the measured current data, however, is approximately linear at higher voltages. The difference between the measured and extrapolated current data indicated a voltage drop which may be due to the Mo/c-BN interface contact resistance (also shown in Fig. 5). A linear fit to the difference of the two currents yielded a contact resistance (R_C) on the order of 9 MΩ. Multiplying R_C by the measured current yields the potential drop across R_C. The data in Fig. 6 show the FEED peak positions after the voltage drop due to the R_C has been taken into account. The shift in FEED peak positions is now approximately linear over the entire measured voltage range, which supports the suggested model that the nonlinearities observed in some FEED spectra were due to a serial contact resistance at the Mo/c-BN interface.

D. Conclusions

In summary, the mechanisms responsible for emission from bare Mo emitters and Mo emitters coated with intrinsic c-BN were investigated through an analysis of V-FEED and I-V measurements. Multiple FEED peaks were observed in the spectra collected from several samples. The energy of field-emitted electrons from c-BN usually depend linearly upon the applied voltage, whereas the energy of electrons field-emitted from bare Mo was not voltage dependent. However, at higher applied voltages, the energy of the field-emitted electrons

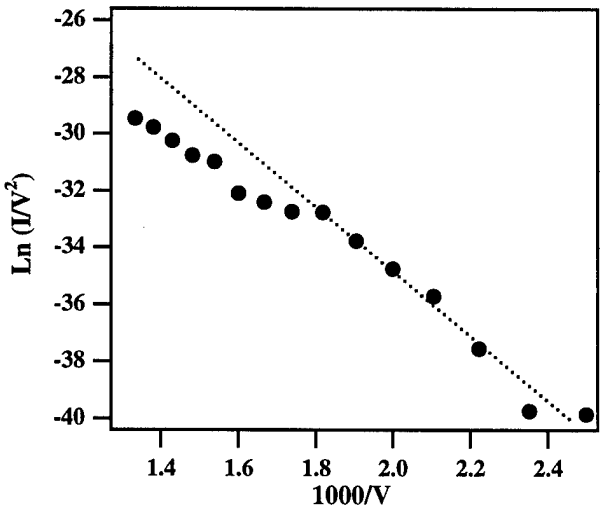

Figure 4. Fowler-Nordheim plot of measured I-V data showing non-ideal behavior. Dashed line represents data extrapolated from lower voltages to higher voltages where the nonlinear behavior was observed.

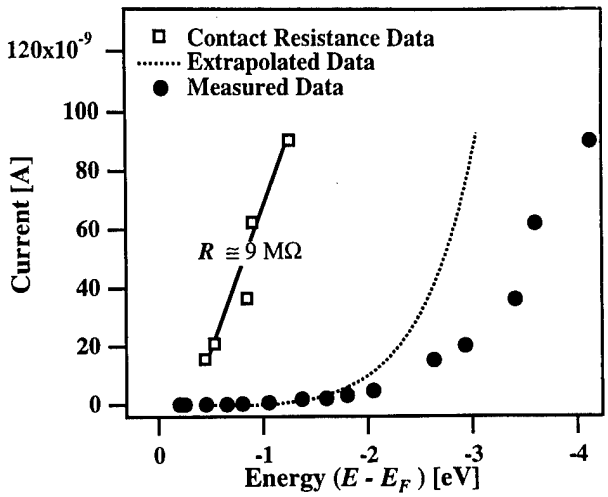

Figure 5. Measured current, extrapolated F-N current, and calculated current loss due to the interfacial contact resistance as a function of FEED peak position. The difference between the extrapolated F-N current data and the measured current data yielded the loss in current and the voltage drop due to the interfacial contact resistance. A linear fit to the contact resistance data produced an average resistance of 9 MΩ.

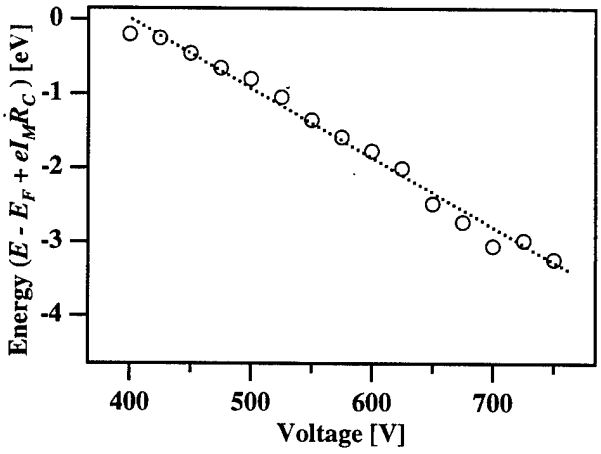

Figure 6. Shift in FEED peak position as a function of the applied voltage after the Mo/c-BN contact resistance (R_C) has been taken into account.

from c-BN was not linearly dependent on the applied voltage and could not be explained with the simplified field-induced band-bending model described previously. Modification of this band-bending model to include the effects of a serial ohmic contact resistance at the Mo/c-BN interface enabled the explanation of this behavior.

E. References

1. C. A. Spindt, J. Appl. Phys. **39**, 3504 (1968).
2. I. Brodie, and C. A. Spindt, Adv. Electron. Electron Phys. **83**, 1 (1992).
3. P. R. Schwoebel, and I. Brodie, J. Vac. Sci. Technol. B **13**, 1391 (1995).
4. W. B. Choi, J. Liu, M. T. McClure, A. F. Myers, V. V. Zhirnov, J. J. Cuomo and J. J. Hren, J. Vac. Sci. Technol. B **14**, 2050 (1996).
5. R. Schlesser, M. T. McClure, W. B. Choi, J. J. Hren, and Z. Sitar, Appl. Phys Lett. **70**, 1596 (1997).
6. R. Schlesser, M. T. McClure, B. L. McCarson, and Z. Sitar, J. Appl. Phys. **82**, 5763 (1997).
7. M. J. Powers, M. C. Benjamin, L. M. Porter, R. J. Nemanich, R. F. Davis, J. J. Cuomo, G. L. Doll, and S. J. Harris, Appl. Phys. Lett. **67**, 3912 (1995).
8. R. W. Pryor, Mat. Res. Soc. Symp. Proc. **416**, 425 (1996).
9. B. L. McCarson, R. Schlesser, M. T. McClure, and Z. Sitar, Appl. Phys. Lett. *in press* (1998).
10. W. B. Choi, A. F. Myers, G. J. Wojak, M. T. McClure, J. J. Cuomo, and J. J. Hren, in Proceedings of the 9th International Vacuum Microelectronics Conference, St.-Petersburg, Russia, July 7-12, 1996, p. 288.

V. Distribution List

Dr. Colin Wood Office of Naval Research Electronics Division, Code: 312 Ballston Tower One 800 N. Quincy Street Arlington, VA 22217-5660	3
Administrative Contracting Officer Office of Naval Research Atlanta Regional Office 100 Alabama Street, Suite 4R15 Atlanta, GA 30303	1
Director, Naval Research Laboratory ATTN: Code 2627 Washington, DC 20375	1
Defense Technical Information Center 8725 John J. Kingman Road, Suite 0944 Ft. Belvoir, VA 22060-6218	2